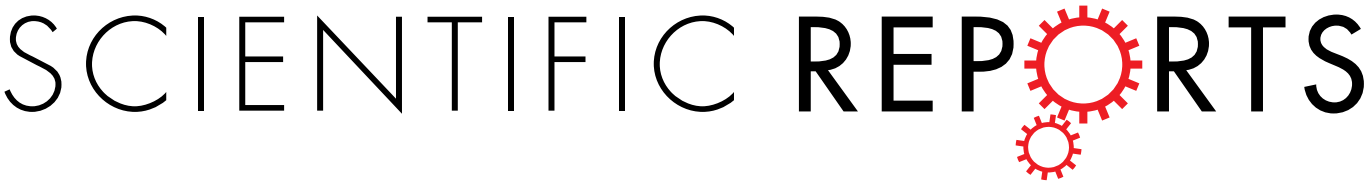

OPEN

Received: 13 October 2015
Accepted: 22 January 2016
Published: 24 February 2016

Scalable Multifunctional Ultra-thin Graphite Sponge: Free-standing, Superporous, Superhydrophobic, Oleophilic Architecture with Ferromagnetic Properties for Environmental Cleaning

Hamed Hosseini Bay[1], Daisy Patino[2], Zafer Mutlu[2], Paige Romero[2], Mihrimah Ozkan[3] & Cengiz S. Ozkan[1,2]

Water decontamination and oil/water separation are principal motives in the surge to develop novel means for sustainability. In this prospect, supplying clean water for the ecosystems is as important as the recovery of the oil spills since the supplies are scarce. Inspired to design an engineering material which not only serves this purpose, but can also be altered for other applications to preserve natural resources, a facile template-free process is suggested to fabricate a superporous, superhydrophobic ultra-thin graphite sponge. Moreover, the process is designed to be inexpensive and scalable. The fabricated sponge can be used to clean up different types of oil, organic solvents, toxic and corrosive contaminants. This versatile microstructure can retain its functionality even when pulverized. The sponge is applicable for targeted sorption and collection due to its ferromagnetic properties. We hope that such a cost-effective process can be embraced and implemented widely.

Over the past decades, alarming consumption of earth's resources and subsequent environmental pollution has raised staid concerns. Frequent oil spills and oil tanker incidents which resulted in catastrophic consequences for marine wild life and ecosystems are evident instances and whistleblowers. To prevent further damage to the environment, novel materials and methods for immediate decontamination and purification of water as well as sustaining the scarce natural resources are most favored. Hence, the research has been converged to adopt and develop new and novel oil sorbent materials[1–5]. A state of the art material for such purpose should have low affinity to water and high oil absorption capacity[6]. In addition, it is expected to cause the least possible harm to the environment and must be reusable[6]. Nonetheless, the proposed structure must be equally inexpensive and scalable to be adopted widely for sustainability[7,8]. Different physical and chemical processes have been foreseen and implemented to engineer such materials with enhanced superhydrophobicity and superoleophilicity as well as high surface area in form of a membrane. The hydrophobicity of graphene foams obtained on a sacrificial nickel foam template was reported to increase dramatically by synthesizing Carbon Nanotubes (CNTs) on graphene foam which physically alters the surface[9,10]. Consequently, the contact angle of water with the structure is changed from 108.5° to 152.3°. However, the porosity of these architectures is limited to macro and hardly ever mesopores. Most recently, promising results have been reported regarding the exceptional oil absorption capacity and recyclability of the CNT and Carbon Nanofiber (CNF) sponges[11,12]. Though these sponges may only be used for a specific purpose which might result in an expensive and challenging transition to industry. Owing to their high surface to volume ratio, very low density and desirable electrical properties as well as chemical and

[1]Department of Mechanical Engineering, University of California, Riverside, CA 92521 USA. [2]Materials Science and Engineering Program, University of California, Riverside, CA 92521 USA. [3]Department of Electrical and Computer Engineering, University of California, Riverside, CA 92521 USA. Correspondence and requests for materials should be addressed to M.O. (email: mihri@ece.ucr.edu) or C.S.O. (email: cozkan@engr.ucr.edu)

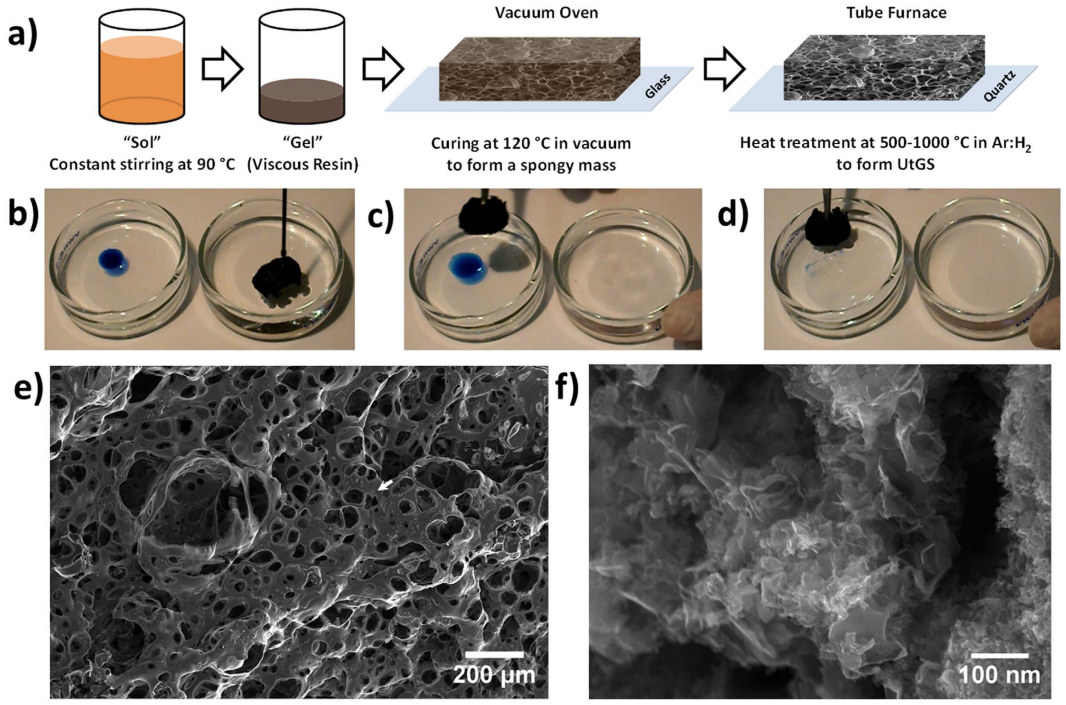

Figure 1. **(a)** Schematic representation of the synthesis **(b)** UtGS on the right container is soaked with toluene dyed with n-blue. **(c)** No leakage of toluene from the sponge to the water is observed. **(d)** UtGS can still clean the toluene spill from the surface of water. **(e)** SEM image of the sponge microstructure. **(f)** High magnification SEM image acquired from the surface of the sponge roughly where the white arrow is pointing at.

mechanical stability, three dimensional (3-D) graphene-based architectures such as foams, sponges and aerogels have been considered as multifunctional viable candidates for oil absorbing materials[10,13]. Additionally, such graphene-based structures are found to be significantly favorable materials for gas sensing[14] and adsorption[15], biological applications[16], thermal management[17], radiation protection and shielding[18], energy conversion and storage[10,15,19,20] and even structural reinforcement[21,22]. Although total surface area of graphene-based sponges must be improved for some specific applications via chemical activation, capitalizing a multifunctional and scalable paradigm is believed to be more practical. The most widely used fabrication process for graphene-based sponges is reported to be hydrothermal reduction and assembly of graphene oxide nanosheets[10,23,24]. Whereas well thought out functionalization of these structures yields tailored assemblies for specific environmental applications[25,26], the hydrothermal process is long and preceded by Hummers method[23,24]. Therefore, characteristics and effectiveness of the sponges strongly depend on a well-established modified Hummers method which is long as well[27]. Herein, to propose a facile, relatively fast and scalable fabrication process, we report the synthesis of a scalable, multifunctional free-standing ultra-thin graphite sponge with superhydrophobic, oleophilic and ferromagnetic properties. The sponge provides an exceptional surface area as well as multimodal porous structure including macro, meso and micropores. In this sense, the structure may be considered as self-activated, and a separate chemical activation to enhance the surface properties is not primarily obligatory. The structure and synthesis process have been thought out to be effortlessly inexpensive and scalable and with minor modifications can be pertinent for different applications.

Synthesis of the Ultra-thin graphite sponge

The Ultra-thin graphite sponge (referred to as UtGS hereafter) is synthesized via a sol-gel process followed by curing and annealing at high temperatures. The synthesis process is shown schematically in Fig. 1(a). A clear, homogeneous aqueous solution of the precursors (sol) was prepared, and a few droplets of nitric acid were added to the solution to adjust the pH at 3 and initiate the polymerization. Under constant stirring at 90 °C, a viscous resin (gel) was formed after a few hours. The viscous resin was spread on a glass substrate and cured in a vacuum oven at 120 °C to form a spongy mass as an intermediate precursor. The spongy precursor was cut to desired shapes with a blade. The UtGS structure was achieved by heat treating the intermediate precursor at high temperatures (500–1000 °C) under argon and hydrogen flow in a horizontal tube furnace.

Characterization of the UtGS sponge

As in Fig. 1(b–d), UtGS can be used to remove toluene from water where toluene is dyed with n-blue dye. In this typical experiment, UtGS sample floating on water was first soaked with toluene droplets (Fig. 1(b)). It appears that toluene is contained within the sponge (Fig. 1(c)), and the soaked sponge can further absorb toluene (Fig. 1(d)). Moreover, supplementary Figure 1 illustrates the separation of chloroform highlighted with 4-(dicyanomethylene)-2-methyl-6-(4-dimethylaminostyryl)-4 H -pyran (DCM), from water. The sequence also exhibits

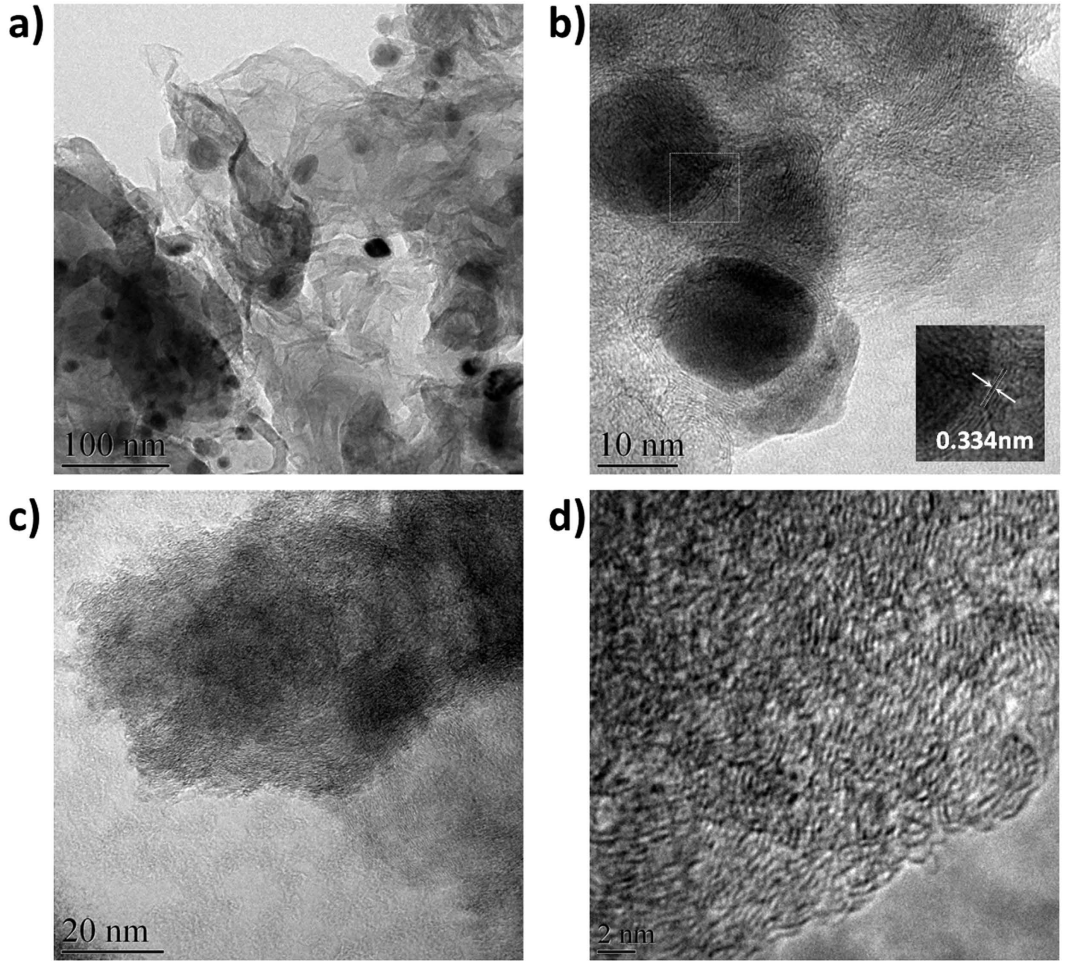

Figure 2. **(a)** Low magnification TEM image of UtGS **(b)** High magnification image of the Fe nanoparticles encapsulated in graphene-based sheets (inset: HRTEM image showing the graphene layers with the interplanar distance highlighted). **(c)** Low magnification image around the surface of UtGS. **(d)** HRTEM image showing the microstructure of the surface of UtGS.

the replacement of air with chloroform within the sponge structure. It appears that UtGS is capable of absorbing organic contaminants with different densities compared to water as well as several dyes and stains from water and also can retain its functionality under water.

To put the recyclability of UtGS to test, a sample was soaked with toluene and then subjected to a flame. The sample containing the absorbed toluene was combusted until all of toluene was consumed. The fire was self-extinguished due to the absence of fuel, and the UtGS sample remained intact and could be used again (supplementary Figure 2(a–c)). Similar studies have been carried out to demonstrate the fire-resistivity and recyclability of graphene-based sponges[28,29]. However, the recovery of the absorbates such as oil and organic solvents from the sorbent after uptake remains a priority. A simple process can be implemented to heat up the UtGS with the contained absorbate to evaporate the absorbed contaminant. The vapor can then be condensed to liquid form and recycled[30]. To further quantify the cyclic recovery, the weight changes of a UtGS sample has been evaluated (supplementary Figure 3). In this instance, the sample was saturated with ethanol and the ethanol was evaporated by annealing at 500 °C for 30 min. UtGS dry weight was accurately consistent within 10 cycles and was measured to be 20.78 mg. UtGS post saturation weight was 469.8 to 471.2 mg and no evident decrease in absorption capacity was observed.

Figure 1(e) reveals the microstructure of the UtGS which appears to be a maze of interconnected macropores. Higher magnification SEM (Fig. 1(f)) shows that the surface of the sponge seems to be very porous and may be considered as possible connected mesopores and channels. Also thin stacks of randomly oriented graphene flakes and layers can be identified on the surface. TEM images reveal that UtGS is consisted of wrinkled and convoluted sheets (multilayer graphene layers) as well as dispersed nanoparticles with average diameter of about 20nm (Fig. 2(a)). Higher magnification TEM imaging demonstrates that iron nanoparticles are encapsulated within the structure by few layers of graphene (Fig. 2(b)). HRTEM images show interplanar distances of 0.34 nm which corresponds to the stacking of sp^2-hybridized layers of carbon (Fig. 2(b) inset). As pointed out in Fig. 2(c), the structure seems to comprise numerous minuscule graphene domains and randomly oriented flakes which attain a

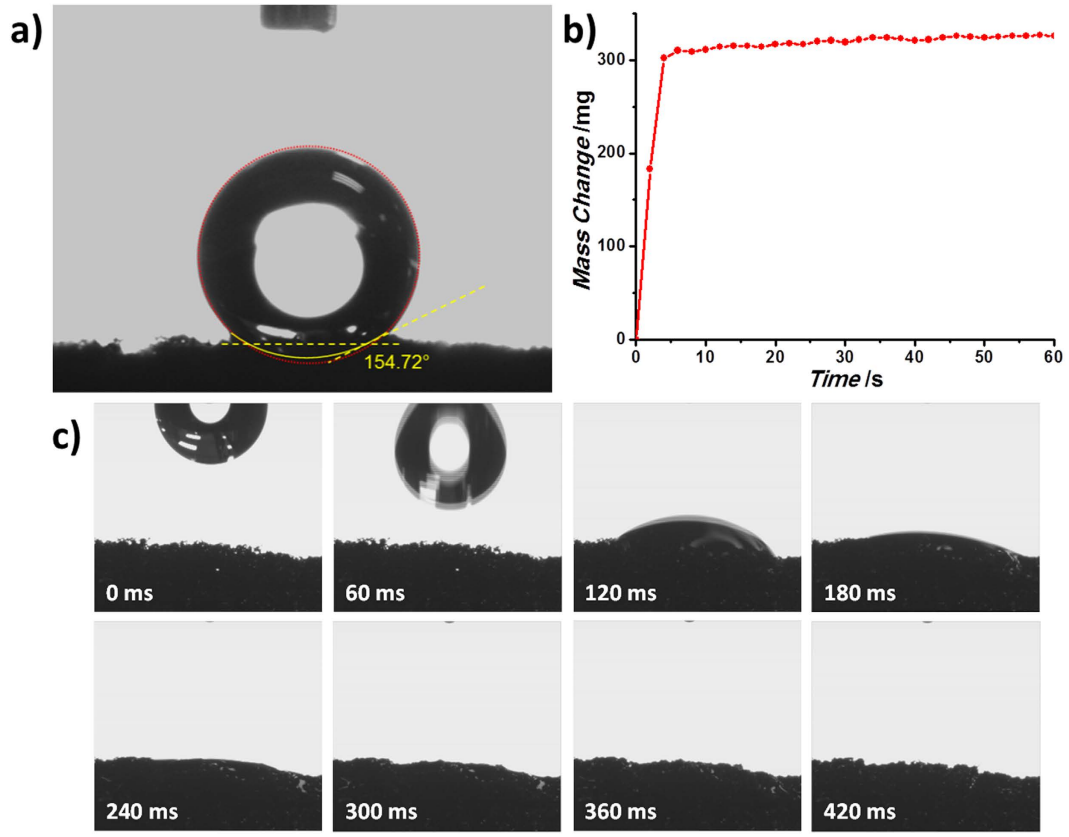

Figure 3. **(a)** Contact angle measurement of UtGS showing superhydrophobicity. **(b)** Graph showing the oil uptake of UtGS with time. (**c**) Snapshots of spreading and absorption of oil by UtGS showing oleophilicity.

rough microstructure encompassing microchannels. HRTEM image resolved from the surface of the sponge indicates the existence of very small graphene-based domains with random orientation and complex stacking as well as sub-nanometer channels separating them (Fig. 2(d)). In this sense, the width of the microchannels separating the graphene domains seems to deviate slightly from the measured interplanar distance of 0.34 nm. HRTEM characterization of UtGS reveals that the interconnected porous structure is supported by graphitic walls consisted of about 10–15 graphene-based layers (supplementary Figure 4). Moreover, measured interplanar spacing of the stacked layers appeared to conform to that of graphitic structures[17].

Figure 3(a) represents the contact angle measurement of water on the sponge which was evaluated to be 154.72°. Such an exceptional hydrophobicity is a result of numerous microscopic and nanoscopic voids of air and surface roughness at the interface with water as well as the possible absence of hydrophilic groups on the surface of the sponge. To investigate the uptake behavior of UtGS structure with time, a sample was exposed to compressor oil, and its weight change was monitored over the course of one minute (Fig. 3(b)). The oil was absorbed into the sponge upon contact and in about 4 to 6 seconds the maximum absorption was reached. To enumerate the absorption capacity ($c = 15.57$) of UtGS, the mass change after oil uptake ($m_f = 327$ mg) is divided by the initial mass ($m_i = 21$ mg) of the sponge. As a result, the maximum weight of compressor oil that can be absorbed by UtGS is about 15.57 times of its weight. Meanwhile, UtGS manifested a similar trend for ethanol sorption (supplementary Figure 5(a)) and the absorption capacity was calculated to be 22.69. Absorption capacities of different organic contaminants are compared in supplementary Figure 5(b) which signifies the complex effect of density, viscosity and surface tension of the absorbate on sorption phenomenon[9]. Figure 3(c) shows snapshots of spreading and absorption behavior of compressor oil in contact with UtGS surface, acquired at 60 millisecond intervals. It reveals that the sponge is oleophilic since the oil is penetrated into the structure upon contact and completely absorbed by the sponge in about 300 ms. Whilst UtGS oil absorption capacity is higher than modified polyurethane foams (about 13.25 $g.g^{-1}$)[3], it is much lower than sorption capacity of CNF aerogels (about 200 $g.g^{-1}$)[12], CNT aerogels (about 125 $g.g^{-1}$)[31], graphene aerogels (about 85 $g.g^{-1}$)[32], and CVD-graphene/CNT hybrid foams (about 90 $g.g^{-1}$)[9]. The porosity of those foams and aerogels is a result of meso- and macro-pores. These 3-D structures also exhibit considerable volume change which contributes to sorption kinetics. UtGS however, offers micro-, meso- and macro-pores at the same time and the high intrinsic surface area of UtGS can be attributed mostly to the meso- and micro-pores. These pores and channels may not contribute to oil absorption due to surface tension restriction of oil which could explain the setback in oil absorption capacity of UtGS compared to CNF, CNT and graphene aerogels. Alternatively, this setback can be compensated by the facile fabrication process, multifunctionality and scalability of UtGS.

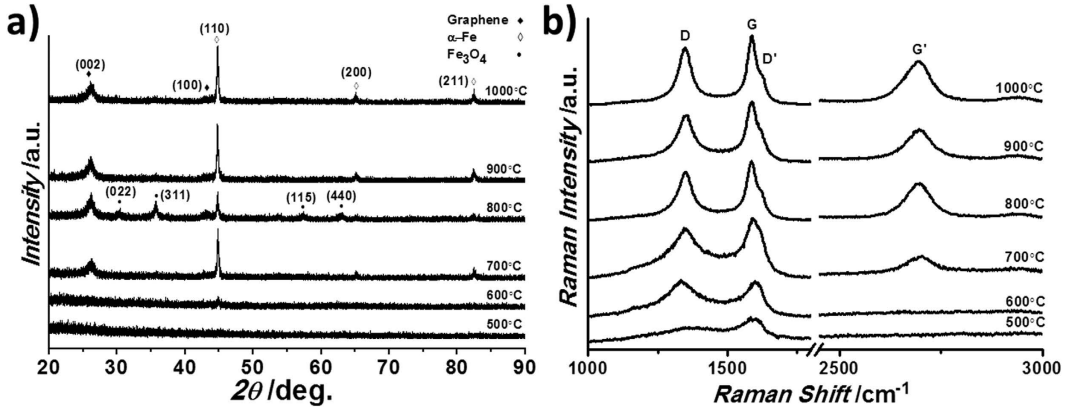

Figure 4. **(a)** XRD multiplot of UtGS heat treated at different temperatures. **(b)** Raman spectra multiplot of UtGS heat treated at different temperatures.

To characterize the details of the microstructure and overlook the structural changes and phase evolutions, X-ray Diffraction (XRD) and Raman spectroscopy have been carried out on UtGS samples prepared at different temperatures. By means of Fig. 4(a), XRD patterns of UtGS samples heat treated at 500, 600, 700, 800, 900 and 1000 °C are demonstrated and compared. According to characteristic diffraction angles, sp^2-hybridized layers in form of graphene as well as α-Fe[33] and Fe_3O_4[33,34] can be identified at different temperatures (Fig. 4(a)). The peak at 24° may correspond to (002) reflection and the peak at 43° can link to superposition of (101) and (100) reflections in sp^2-hybridized graphitic lattice structure[35]. It has been reported by other researchers that these two peaks can be related to graphene sheets and flakes[36–39]. In addition, syntheses at higher temperatures yield to higher crystallinity of the structure since the XRD peaks appear to be sharper with higher relative intensities. As seen in Fig. 2(a,b), it is most likely that the dispersed nanoparticles in the microstructure are α-Fe nanoparticles with diameter of about 20 nm. While some of these nanoparticles are encapsulated with few layers of graphene, some nanoparticles can be found unprotected on the surface of the sponge. It is critical to note that the final heat treatment of the sponge precursor is done under argon and hydrogen atmosphere which prevents the oxidation of Fe nanoparticles. Nevertheless, as soon as the sponge is removed from the reducing environment of the furnace and subjected to air, the nanoparticles are highly prone to surface oxidation. Consequently, trace of Fe_3O_4 is observed in the XRD pattern from 700 °C (Fig. 4(a)). Supplementary Figure 6(a),(b) represent the Energy Dispersive X-ray Spectroscopy (EDS) spectra of an untreated UtGS sample and a sample treated with hydrochloric acid (HCl), respectively. As a result of acid treatment, the amount of Fe in the structure was decreased from 12.69 to 5.55 wt% by dissolving the unprotected Fe nanoparticles. Therefore, about 5.55 wt% of the structure is believed to be graphene wrapped α-Fe nanoparticles. To complement this assessment, the untreated UtGS sample has been subjected to a mixture of C_2H_4:H_2 to synthesize carbon nanotubes (CNTs) using the iron nanoparticles as catalysts. Supplementary Figure 6(c),(d) demonstrate that multi-walled CNTs of various diameters encompassing iron nanoparticles at their tip can be originated on the surface of the sponge. As an exhibit for its versatility and multifunctionality, UtGS may be used for facile fabrication of free-standing 3-D graphene-CNT hybrid architectures.

Figure 4(b) shows Raman spectra of UtGS heat treated at different temperatures. Three characteristic Raman peaks of graphene, D, G and G', respectively at 1335, 1580 and 2680 cm^{-1} can be observed in the spectra[40]. Since G' peak of graphite is believed to be asymmetric and splitted into four peaks[41,42], the peak centered at about 2680 cm^{-1} can be associated to G' peak of graphene. The broad D peak in the spectra infers the high level of disorder in structure. To investigate the changes in the UtGS structure, D to G (I_D/I_G) and G' to G ($I_{G'}/I_G$) peak intensity ratio at different heat treatment temperatures have been plotted separately in supplementary Figure 7. As the temperature ramps up, I_D/I_G which refers to the disorder in graphene layers, follows a general ascending trend except from 600 to 700 °C, where it plummets. Similarly, $I_{G'}/I_G$ as a measure for the number of stacked graphene layers, increases with temperature. It seems that the formation of graphene-based sheets starts at about 700 °C, since G' peak emerges at this temperature. Evolution of the system from 600 to 700 °C can be interpreted as incubation for amorphous to crystalline transition. Since the graphene-based sheets are starting to nucleate and grow, the degree of disorder seems to drop temporarily. Afterwards, the formation of the spatially convoluted graphene sheets yields to higher degree of disorder. The ascending trend of $I_{G'}/I_G$ implies that the growing graphene layers are not stacking or possibly forming a turbostratic structure, where the stacked layers are slipped sideways relative to one another to create microchannels[43]. The presence of D' peak at 1608 cm^{-1}, accentuates high degree of disorder in graphene domains and also convey that graphene-based sheets may have been doped with nitrogen[44].

In order to investigate the chemical reactions and alterations of the precursors during the synthesis process, Fourier Transform Infrared (FTIR) spectroscopy has been performed on the cured resin. FTIR results (Fig. 5(a)) display a broad peak at 3398cm^{-1} due to stretching vibrations of O-H bonds[45]. Weak bands appeared at 2920 and 2879 cm^{-1} correspond to the symmetric and asymmetric vibrations of C-H bonds[46] and the bands at 1718 and 1622 cm^{-1} are due to C=O and C=C bonds stretching vibrations respectively[45,47]. Narrow band at about 1405 cm^{-1} correlates O-H bond bending vibrations[45], and the peaks at about 1350 cm^{-1} occur as a result of C-OH bond stretching vibrations[48]. C-N bond stretching vibrations as well as breathing vibrations of epoxy groups may be attributed to the peaks at about1200 cm^{-1}[49]. Vibrations at about 1050–1070 cm^{-1} can be related to stretching

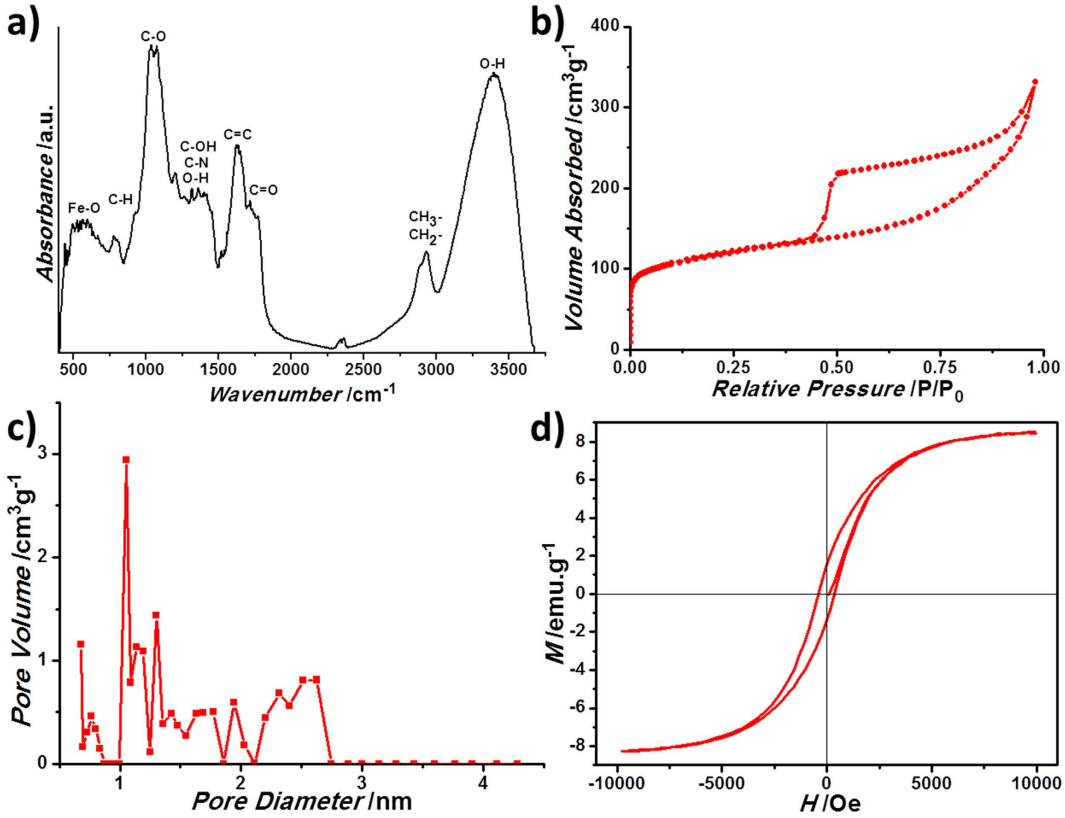

Figure 5. **(a)** FTIR spectrum of UtGS precursor after curing and before final heat treatment. **(b)** BET surface area measurement of UtGS with a combination of type I and type IV N_2 sorption. **(c)** Pore size distribution of UtGS (calculated based on DFT model). **(d)** Magnetic hysteresis loop curve acquired from UtGS.

vibrations of C-O bonds[45,46]. Further trace of C-H bonds can be seen at 932 cm^{-1} as out of plane vibration bands[49]. Bands between 480 to 730 cm^{-1} are suggested to be related to Fe-O stretching vibrations[47,49]. The chemistry of the sol-gel process is schematically illustrated in Supplementary Figure 8. It looks as if during the sol-gel process, hydrolysis of sucrose followed by addition of nitric acid results in the formation of saccaric acid[50,51]. Simultaneous reaction of PVA monomers and iron cations with saccaric acid at 90 °C first originates long chains of polymeric resin and later yields to cross linking of the chains to convert the sol to a gel[50,51]. These long chains in the gel have accommodated iron cations, and they seem to contain all of the aforementioned bonds which have been identified in the FTIR measurement. It is likely that heat treatment at high temperatures dissociates the bonds between carbon with hydrogen, oxygen and nitrogen and allows them to leave the structure in form of gas molecules. This may also aid the formation of the microchannels and the possible turbostratic structure of the graphene-based sheet. The heat treatment also results in decomposition of the hydrophilic groups on the surface of the sponge which in its term contributes to hydrophobicity. While the structure is being carbonized at high temperatures in a reducing atmosphere, neighboring iron cations will cluster and form iron nanoparticles. As an example for the adaptability of UtGS, a similar modified sol-gel process has been reported for the synthesis of metal oxides which implies the possibility to incorporate other metallic nanoparticles in the structure upon designated applications[50,51].

Brunauer–Emmett–Teller (BET) surface area measurements have been carried out to quantify the surface area and porosity of UtGS architecture. Figure 5(b,c) summarize the results of adsorption-desorption isotherms and BET pore size distribution, respectively. It seems that the structure exhibits a combination of type I and type IV N_2 adsorption-desorption isotherms[52,53]. The adsorption in relative pressures less than about 0.1 implies that micropors or microchannels can be found in the sample, whereas the hysteresis loop from relative pressures of about 0.5 to 1.0 is related to the mesopores[54]. The average pore diameter was calculated using DFT model to be about 1.4 nm. The Langmuir and BET surface area of UtGS sample were measured to be 1356.30 and 823.77 $m^2.g^{-1}$, respectively which implies that there will be no predominant concern for chemical activation in order to enhance porosity and surface area. Besides, the density of UtGS was calculated to be 0.017 $gr.cm^{-3}$. It may be inferred that the majority of the surface area should be attributed to the micropores and microchannels. Nonetheless, this cannot contradict the actuality and contribution of the mesopores which can be identified in high magnification SEM image (Fig. 1(e)). While the mesopores may contain a portion of the total volume of the condensate, the amount of micropores and microchannels significantly prevails. Thus mesopores do not contribute to the pore distribution as might be expected[55]. Supplementary Figure 9(a) through (e) represents the snapshots taken during an experiment designed to qualitatively evaluate the effectiveness of pulverized UtGS. The pulverized sample was poured into a container of water contaminated by ethanol dyed with rhodamine b. A magnet was placed inside

the container to collect the sponge powder. The collected sample seems to absorb the contamination effectively, as there was no trace of rhodamine b (pink dye dissolved in ethanol). Supplementary Figure 9(f,g) give an idea about the size of the particles; and show high magnification SEM image of a fractured cross-section to depict the porosity within the bulk of UtGS, respectively. In this sense, the absorption of the contaminants may be attributed to the meso and micropores. Congregated graphene-based layers and exposed iron nanoparticles as well as meso-channels and pores can be envisioned within the cross section of the pulverized sponge particles (Supplementary Figure 9(g)).

To further demonstrate the versatility of G-sponge, the viscous resin was cured while a constant flow of nitrogen was used to generate bubbles in the resin, the microstructure was affected as shown with different magnifications in Supplementary Figure 10(a),(b). It seems that this process prompts macropore formation as opposed to mesopores, since the surface seems to be less porous (Supplementary Figure 10(b)). Conversely, when curing was done under nitrogen pressure, a conformal layered structure was formed after annealing at high temperatures (Supplementary Figure 10(c),(d)) as if the crosslinking of the resin chains was suppressed under pressure.

The magnetic hysteresis loop of UtGS is demonstrated in Fig. 5(d) and conforms to that of ferromagnetic materials[56]. The saturation magnetism (M_S) and the coercivity (H_C) have been measured to be 8.49 emu.g^{-1} and 336 Oe at room temperature. Hence, α-Fe nanoparticles may accommodate single magnetic domains, due to the high measured H_C and the average diameter of the particles (20 nm)[56]. The measured M_S is relatively small compared to the reported values for α-Fe nanoparticles with similar size since it is only 12.69% of the total weight. Relating back to XRD multiplot shown in Fig. 4(a), at 500 and 600 °C no or minute traces of α-Fe was observed which points out that ferromagnetism may not be observed in the samples heat treated bellow 600 °C. The ferromagnetic properties can offer selectivity for targeted delivery and collection of the sponge.

Conclusions

In summary, we have successfully demonstrated the synthesis of a scalable, multifunctional ultra-thin graphite sponge with exceptional porosity and surface area as well as superhydrophobic and oleophilic properties via a modified sol-gel assisted process. The structure and synthesis process are designed to be effortlessly inexpensive and highly scalable to be widely adopted and used. The synthesized sponge has ferromagnetic properties as a result of graphene-wrapped α-Fe nanoparticles with average diameter of about 20 nm. We have also illustrated the versatility of the architecture enabling the required modifications such as direct CNT growth or incorporation of other metallic nanoparticles within the structure which expands its applicable venues. The obtained sponge has an exceptional contact angle of 154.72° with water as well as oleophilic properties. It offers a remarkable surface area of 823.77 m^2.g^{-1} and an average pore diameter of 1.4 nm without chemical activations. Such surface area is due to the presence of macro, meso and micropores and channels in the structure. The sponge is effectively applicable to be used underwater and even when pulverized. Selective and targeted delivery and collection of the sponge to contaminated coordinates is also possible as a result of embedded ferromagnetic α-Fe nanoparticles. The achieved architecture offers a promising ability environmental cleaning applications such as oil-water separation and water decontamination. Owing to its versatile microstructure, it may also be used for gas filtration and sensing as well as energy storage.

Methods

Synthesis of the UtGS. UtGS was prepared by a modified sol-gel process followed by curing in vacuum and annealing at high temperature. Briefly, 2.82 g sucrose (Sigma-Aldrich, >99.5%), 0.12 g polyvinyl alcohol (Sigma-Aldrich, 98–99%) and 0.84 g iron nitrate nonahydrate (Sigma-Aldrich, >98%) were dissolved in 17 ml deionized (DI) water and stirred to form a homogenous solution. 0.1 ml nitric acid (HNO_3) was added to the final solution (sol), and the temperature was then raised up to 90 °C for 1 hour. A viscous dark brown resin (gel) was formed as a result of a series of chemical reactions and polymerization. The resin was cured at 120 °C under vacuum for 2 hours. Then the cured resin was cut into the desired shapes with a blade and transferred into a horizontal tube furnace. The temperature was ramped up with a rate of 10 °C.min^{-1} to the final temperature (500, 600, 700, 800, 900 and 1000 °C). The samples were annealed at 5 torr for 30 minutes in Ar and H_2 atmosphere with the flow rates of 100 and 50 sccm, respectively to form the final sponge structure.

Absorption capacity measurements of UtGS. To evaluate the kinetic sorption behavior, a 1:1 ratio of deionized (DI) water and contaminant was used. UtGS samples were placed on the surface of water and weighed at different times upon absorption. The measurements continued until a plateau of weight change was achieved. Each set of measurements repeated eight times.

To measure the absolute absorption capacity, UtGS samples were submerged in a container of contaminant and sonicated for 10 minutes. Each set of measurements repeated 8 times.

Synthesis of CNTs on UtGS. The CNTs were grown on UtGS via Chemical Vapor Deposition (CVD) method in a horizontal tube furnace using the Fe nanoparticles on the surface of UtGS as catalyst. A mixture of Ar, H_2 and ethylene (as carbon precursor) were flowed with the rate of 150,100 and 50 sccm, respectively. The temperature was ramped up with a rate of 10 °C.min^{-1} to 750 °C and, the growth was done at 700 torr for 30 minutes.

Acid treatment to remove Fe nanoparticles. UtGS samples were sonicated overnight in a mixture of ethanol and HCl with the ratio of 1:1 by volume. The acid treated samples were sonicated and washed several times with absolute ethanol until the neutral pH was achieved and dried overnight under vacuum at 90 °C.

Materials characterization. The morphology investigation and imaging analysis were performed using scanning electron microscope (SEM; FIB NNS450) equipped with X-ray energy dispersive spectroscopy (EDS)

and transmission electron microscope (TEM; Philips, CM300) with a LaB_6 cathode operated at 300 KV. For TEM imaging, the pulverized sponge was dispersed ultrasonically in ethanol for 1 hour, and a diluted sample was drop casted on the carbon-coated TEM grid. Crystal structure and phase identification was done by X-ray diffraction analysis (XRD, Philips X′Pert) using Cu Kα radiation. Raman spectrum was collected using a Horiba LabRAM HR spectrometer and an excitation source with wavelength of 532 nm. Fourier transform infrared spectroscopy was carried out using a Bruker Equinox 55 FTIR. The surface area and pore size distribution analysis were accomplished by means of Brunauer-Emmett-Teller (BET) measurements using Micromeritics ASAP 2020 with nitrogen gas. Magnetic properties were measured using a vibrating sample magnetometer (VSM).

References

1. Feng, X. *et al.* Design and creation of superwetting/antiwetting surfaces. *Adv. Mater.* **18,** 3063–3078 (2006).
2. Feng, L. *et al.* A super-hydrophobic and super-oleophilic coating mesh film for the separation of oil and water. *Angew. Chemie - Int. Ed.* **43,** 2012–2014 (2004).
3. Calcagnile, P. *et al.* Magnetically driven floating foams for the removal of oil contaminants from water. *ACS Nano* **6,** 5413–9 (2012).
4. Yao, X. *et al.* Applications of bio-inspired special wettable surfaces. *Adv. Mater.* **23,** 719–734 (2011).
5. Thanikaivelan, P. *et al.* Collagen based magnetic nanocomposites for oil removal applications. *Sci. Rep.* **2,** 230 (2012).
6. Chu, Y. *et al.* Three-dimensionally macroporous Fe/C nanocomposites as highly selective oil-absorption materials. *ACS Appl. Mater. Interfaces* **4**, 2420–2425 (2012).
7. Yang, Z. Y. *et al.* Sponge-templated preparation of high surface area graphene with ultrahigh capacitive deionization performance. *Adv. Funct. Mater.* **24,** 3917–3925 (2014).
8. Mohan, D. *et al.* Organic and inorganic contaminants removal from water with biochar, a renewable, low cost and sustainable adsorbent - A critical review. *Bioresour. Technol.* **160,** 191–202 (2014).
9. Dong, X. *et al.* Superhydrophobic and superoleophilic hybrid foam of graphene and carbon nanotube for selective removal of oils or organic solvents from the surface of water. *Chem. Commun. (Camb).* **48,** 10660–2 (2012).
10. Li, Z. *et al.* Superstructured Assembly of Nanocarbons: Fullerenes, Nanotubes, and Graphene. *Chem. Rev.* **115,** 7046–7117 (2015).
11. Gui, X. *et al.* Recyclable carbon nanotube sponges for oil absorption. *Acta Mater.* **59,** 4798–4804 (2011).
12. Bi, H. *et al.* Carbon fiber aerogel made from raw cotton: A novel, efficient and recyclable sorbent for oils and organic solvents. *Adv. Mater.* **25,** 5916–5921 (2013).
13. Sun, H. *et al.* Multifunctional, ultra-flyweight, synergistically assembled carbon aerogels. *Adv. Mater.* **25,** 2554–2560 (2013).
14. Yavari, F. *et al.* High Sensitivity Gas Detection Using a Macroscopic Three-Dimensional Graphene Foam Network. *Sci. Rep.* **1,** 1–5 (2011).
15. Robertson, C. *et al.* Microporous activated carbon aerogels via a simple subcritical drying route for CO_2 capture and hydrogen storage. *Microporous Mesoporous Mater*. **179,** 151–156 (2013).
16. Li, N. *et al.* Three-dimensional graphene foam as a biocompatible and conductive scaffold for neural stem cells. *Sci. Rep.* **3,** 1604 (2013).
17. Pettes, M. T. *et al.* Thermal transport in three-dimensional foam architectures of few-layer graphene and ultrathin graphite. *Nano Lett.* **12,** 2959–2964 (2012).
18. Chen, Z. *et al.* Lightweight and flexible graphene foam composites for high-performance electromagnetic interference shielding. *Adv. Mater.* **25,** 1296–1300 (2013).
19. Luo, J. *et al.* Three-dimensional graphene foam supported Fe_3O_4 lithium battery anodes with long cycle life and high rate capability. *Nano Lett.* **13,** 6136–43 (2013).
20. Xue, Y. *et al.* Nitrogen-doped graphene foams as metal-free counter electrodes in high-performance dye-sensitized solar cells. *Angew. Chemie - Int. Ed.* 51, 12124–12127 (2012).
21. Li, Y. *et al.* Highly compressible macroporous graphene monoliths via an improved hydrothermal process. *Adv. Mater.* **26,** 4789–4793 (2014).
22. Wu, Y. *et al.* Three-dimensionally bonded spongy graphene material with super compressive elasticity and near-zero Poisson's ratio. *Nat. Commun.* **6,** 6141 (2015).
23. Lu, S. *et al.* Three-dimensional sulfur/graphene multifunctional hybrid sponges for lithium-sulfur batteries with large areal mass loading. *Sci. Rep*. **4,** 4629 (2014).
24. Xu, Y. *et al.* Self-assembled graphene hydrogel via a one-step hydrothermal process. *ACS Nano* **4,** 4324–4330 (2010).
25. Shen, Y. *et al.* Environmental Applications of Three-Dimensional Graphene-Based Macrostructures : Adsorption , Transformation, and Detection. *Environ. Sci. Technol.* **49(1),** 67–84 (2015).
26. Kemp, K. C. *et al.* Environmental applications using graphene composites: water remediation and gas adsorption. *Nanoscale* **5,** 3149–71 (2013).
27. Marcano, D. C. *et al.* Improved Synthesis of Graphene Oxide. *ACS Nano* **4,** 4806–4814 (2010).
28. Qiu, S. *et al.* Hydrophobic and fire-resistant carbon monolith from melamine sponge: A recyclable sorbent for oil–water separation. *Carbon N. Y.* **84,** 551–559 (2015).
29. Zhao, Y. *et al.* A versatile, ultralight, nitrogen-doped graphene framework. *Angew. Chemie - Int. Ed.* **51,** 11371–11375 (2012).
30. Wu, Z.-Y. *et al.* Carbon nanofiber aerogels for emergent cleanup of oil spillage and chemical leakage under harsh conditions. *Sci. Rep.* **4,** 1–6 (2014).
31. Gui, X. *et al.* Carbon nanotube sponges. *Adv. Mater.* **22,** 617–621 (2010).
32. Chabot, V. *et al.* A review of graphene and graphene oxide sponge: material synthesis and applications to energy and the environment. *Energy Environ. Sci.* **7,** 1564 (2014).
33. Wu, W. *et al.* Void coalescence in core/alloy nanoparticles with stainless interfaces. *Small* **10,** 271–276 (2014).
34. Peng, S. *et al.* Synthesis and characterization of monodisperse hollow Fe_3O_4 nanoparticles. *Angew. Chem. Int. Ed. Engl.* **46,** 4155–4158 (2007).
35. Xu, J. *et al.* Preparing two-dimensional microporous carbon from Pistachio nutshell with high areal capacitance as supercapacitor materials. *Sci. Rep*. **4,** 1–6 (2014).
36. Chen, H. *et al.* Mechanically strong, electrically conductive, and biocompatible graphene paper. *Adv. Mater.* **20,** 3557–3561 (2008).
37. Fan, Z.-J. *et al.* Facile synthesis of graphene nanosheets via Fe reduction of exfoliated graphite oxide. *ACS Nano* **5,** 191–198 (2011).
38. Fan, Z. *et al.* A three-dimensional carbon nanotube/graphene sandwich and its application as electrode in supercapacitors. *Adv. Mater.* **22,** 3723–3728 (2010).
39. Zheng, F. *et al.* High lithium anodic performance of highly nitrogen-doped porous carbon prepared from a metal-organic framework. *Nat. Commun.* **5,** 5261 (2014).
40. Ferrari, A. C. Raman spectroscopy of graphene and graphite: Disorder, electron-phonon coupling, doping and nonadiabatic effects. *Solid State Commun.* **143,** 47–57 (2007).
41. Ferrari, A. C. *et al.* Raman spectrum of graphene and graphene layers. *Phys. Rev. Lett.* **97,** 1–4 (2006).
42. Ferrari, A. C. *et al.* Raman spectroscopy as a versatile tool for studying the properties of graphene. *Nat. Nanotechnol.* **8,** 235–46 (2013).

43. Cai, J. *et al.* Large surface area sucrose-based carbons via template-assisted routes: Preparation, microstructure, and hydrogen adsorption properties. *Colloids Surfaces A Physicochem. Eng. Asp.* **444,** 240–245 (2014).
44. Luo, Z. *et al.* Pyridinic N doped graphene: synthesis, electronic structure, and electrocatalytic property. *J. Mater. Chem.* **21,** 8038 (2011).
45. Huang, S. *et al.* Preparation of graphene/Co_3O_4 composites by hydrothermal method and their electrochemical properties. *Electrochim. Acta* **95,** 139–145 (2013).
46. Li, B. *et al.* Superparamagnetic Fe_3O_4 nanocrystals@graphene composites for energy storage devices. *J. Mater. Chem.* **21,** 5069 (2011).
47. Dong, Y. *et al.* Graphene oxide–Fe_3O_4 magnetic nanocomposites with peroxidase-like activity for colorimetric detection of glucose. *Nanoscale* **4,** 3969 (2012).
48. Lee, J. W. *et al.* Hydrothermal preparation of nitrogen-doped graphene sheets via hexamethylenetetramine for application as supercapacitor electrodes. *Electrochim. Acta* **85,** 459–466 (2012).
49. Wang, Y. *et al.* Synthesis of orange-like Fe_3O_4/PPy composite microspheres and their excellent Cr(vi) ion removal properties. *J. Mater. Chem.* **22,** 9034 (2012).
50. Beitollahi, A. *et al.* Synthesis and characterization of Al_2O_3–ZrO_2 nanocomposite powder by sucrose process. *J. Mater. Sci. Mater. Electron.* **21,** 130–136 (2010).
51. Das, R. N. Nanocrystalline ceramics from sucrose process. *Mater. Lett.* **47,** 344–350 (2001).
52. Sing, K. S. W. *et al.* International union of pure commission on colloid and surface chemistry including catalysis * Reporting physisorption data for gas/solid systems with Special Reference to the Determination of Surface Area and Porosity. *Pure Appl. Chem.* **57,** 603–619 (1985).
53. Muniandy, L. *et al.* The synthesis and characterization of high purity mixed microporous/mesoporous activated carbon from rice husk using chemical activation with NaOH and KOH. *Microporous Mesoporous Mater.* **197,** 316–323 (2014).
54. Yin, J. *et al.* Meso- and micro- porous composite carbons derived from humic acid for supercapacitors. *Electrochim. Acta* **136,** 504–512 (2014).
55. Halenda, P. *et al.* The Determination of Pore Volume and Area Distributions in Porous Substances. I. Computations from Nitrogen Isotherms. *J. Am. Chem. Soc.* **73(1),** 373–380 (1951).
56. Huber, D. L. Synthesis, properties, and applications of iron nanoparticles. *Small* **1,** 482–501 (2005).

Author Contributions

H.H.B., M.O. and C.S.O. designed the experiments. H.H.B. and D.P. conducted the material synthesis. H.H.B. designed and supervised all characterizations. Material Characterizations were done by H.H.B., D.P., Z.M. and P.R. H.H.B. analyzed the data. H.H.B., M.O. and C.S.O. wrote the manuscript. C.S.O. and M.O. managed the research team. All authors reviewed the manuscript.

Additional Information

Supplementary information accompanies this paper at http://www.nature.com/srep

Competing financial interests: The authors declare no competing financial interests.

How to cite this article: Bay, H. H. *et al.* Scalable Multifunctional Ultra-thin Graphite Sponge: Free-standing, Superporous, Superhydrophobic, Oleophilic Architecture with Ferromagnetic Properties for Environmental Cleaning. *Sci. Rep.* **6**, 21858; doi: 10.1038/srep21858 (2016).